

Simulation of Rotational Flows in Cylindrical Vessel with Rotating Single Stirrer

A. Baloch

M. A. Solangi

Department of Basic Sciences and Related Studies
Mehran University of Engineering and Technology
Jamshoro, Pakistan.

G. M. Memon

Department of Mathematics
Shah Abdul Latif University
Khairpur Mirs, Pakistan.

Abstract. The purpose of this research is to investigate the influence of rotational speed and rotational direction of stirrer on the hydrodynamics and compare behavior against previously simulated numerical results in the dissolution vessel with fixed stirrer. The numerical simulation of two-dimensional incompressible complex flows of Newtonian fluid passed a stationary and rotating single stirrer within a cylindrical vessel is presented. The context is one, relevant to the food industry, of mixing fluid within a cylindrical vessel, where stirrer is located on the lid of the vessel eccentrically configured. Here, the motion is considered as driven by the rotation of the outer vessel wall, with various rotational speeds of vessel and stirrer. The numerical method adopted is based on a finite element semi-implicit time-stepping Taylor-Galerkin/pressure-correction scheme, posed in a cylindrical polar coordinate system. Numerical solutions are sought for Newtonian fluid. Variation with increasing speed of vessel, change in speed of stirrer and change in rotational direction of stirrer in mixer geometry are analysed, with respect to the flow structure and pressure drop.

Key Words: Numerical Simulation, Finite Element Method, Mixing Flows, Newtonian Fluids, Rotating Flow, Co-rotating Stirrer, Contra-rotating Stirrer.

1. INTRODUCTION

The rotational mixing in stirred vessel for the optimal design is of industrial importance, usually industrial problems are much harder to tackle, particularly in the field of chemical process applications, such as powder mixing processes [1], granular mixing, mixing of paper pulp in paper industry, mixing of dough in a food processing industry [2, 3] and many other industrial processes. In many mixing

processes the complicating factors are the use of the fluids which exhibits very complex rheological behavior, the use of agitators with stirrer in fact that the agitator may be operated in the transitional regime and the direction of rotational speed of stirrer. The present problem is one of this form, expressed as the flow between an outer rotating cylindrical vessel wall and a single stationary and rotating cylindrical stirrer in both co-rotating and contra-rotating directions. Stirrer is located on the mixing vessel lid, and placed in an eccentric position with respect to the central cylindrical axis of the vessel. Under two-dimensional assumptions, the vessel essentially is considered to have infinite height. Elsewhere, the finite vessel problem in three-dimensions [3]-[7] has been analysed. In two-dimension, similar problem is also investigated with different number and shapes of stirrers [8, 9]. The motivation for this work is to advance fundamental technology modelling of the dough kneading with the ultimate aim to predict the optimal design of dough mixers themselves, hence, leading to efficient dough processing.

This problem has similarity to the classical journal bearing problem, associated with lubrication theory, involving a degree of eccentricity between outer and inner cylinders. The journal bearing problem has been solved for viscoelastic fluids employing finite element methods [10, 11] and spectral element methods [12]. Dris and Shaqfeh [10, 11] with finite elements, observed purely elastic flow instabilities in eccentric cylinder flow geometries. The velocity profiles vary as a function of eccentricity, azimuthal coordinate, and the ratio of cylindrical rotation rates. The local flow dynamics span over the entire range of flows from Taylor-Couette flow to Dean flow. The onset of flow instabilities has been shown to be the result of non-local effects in the flow [10]. Global effects drastically alter the hoop stresses in the base flow.

The present study adopts a semi-implicit Taylor-Galerkin/Pressure-Correction (TGPC) finite element time-marching scheme, which has been developed and refined over the last two decades. This scheme, initially conceived in sequential form, is appropriate for the simulation of incompressible Newtonian flows [14]-[17].

In Section 2, the complete problem is specified and the governing equations are described in Section 3. This is followed, in Section 4, by an outline of the TGCP numerical method employed for the simulations. Simulation results are presented in Section 5 and our conclusions are drawn in Section 6.

2. PROBLEM SPECIFICATION

The problem investigated here is two-dimensional mixing flows of Newtonian fluids, of relevance to the food industry such as occurs in dough kneading. Such flows are rotating, driven by the rotation of the outer containing cylindrical-shaped vessel. The stirrer is held in place by being attached to the lid of the vessel. In reality, within the industrial process, the lid of the vessel would rotate with stirrer attached. With a single stirrer, an eccentric configuration is adopted.

Initially, the problem is analysed for rotating flow between stationary stirrer in rotating cylindrical vessel, to validate the finite element discretisation in this cylindrical polar co-ordinate system to compare the numerical results against results obtained in previous investigations [7, 8]. Subsequently, two alternative rotational directions (Co-rotating and contra-rotating) of stirrer are investigated in a rotating cylindrical vessel. Throughout Newtonian fluid is considered.

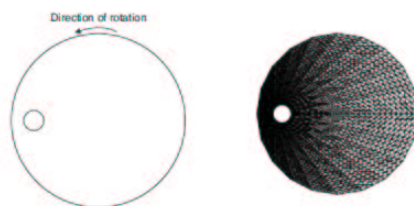


FIGURE 1. Eccentric rotating cylinder flow, with one stationary and rotating stirrer; Domain and finite element mesh

Domain and finite element mesh for the problem involved is displayed in Figure-1. In pervious investigations [7, 8], for mesh convergence studies, three meshes were generated, adopting a hierarchical mesh refinement technique. In this technique, each parent element of the coarser mesh is divided into four child elements. Between the solutions of any variable on two consecutive refined meshes, a discrepancy of order one percent tolerance was fixed. Due to enhancement in power of computation and based on pervious findings, the refined mesh M3 [7] is reasonably adoption for smooth and accurate solutions. The total number of elements, nodes and degrees-of-freedom are 3840, 7840 and 17680 respectively.

To provide a well-posed specification for each flow problem, it is necessary to prescribe appropriate initial and boundary conditions. Simulations commence from a quiescent initial state. Boundary conditions are taken as follows. For stationary stirrer the fluid may stick to the solid surfaces, so that the components of velocity vanish on the solid inner stirrer sections of the boundary ($v_r = 0$ and $v_\theta = 0$). For non-stationary stirrer, fixed constant velocity boundary conditions are applied. For co-rotating stirrer, vanishing radial velocity component ($v_r = 0$) is fixed and for azimuthal velocity component is fixed with three different non-dimensional speeds ($v_\theta = 0.5, 1$ and 2 unit). Similarly, for contra-rotating stirrer only azimuthal velocity component is changed and fixed in reverse direction (i.e., $v_\theta = -0.5, -1$ and -2 unit). On the outer rotating cylinder vessel a fixed constant velocity boundary condition is applied ($v_r = 0$ and $v_\theta = 1$ unit), and a pressure level is specified as zero for both co-rotating and contra-rotating stirrer on vessel wall. For stream function, outer cylinder is fixed zero and at inner stirrer is left unconstrained, being solutions on closed streamlines.

3. GOVERNING SYSTEM OF EQUATIONS

The two-dimensional isothermal flow of incompressible Newtonian fluid can be modelled through a system comprising of the generalised momentum transport and conservation of mass equations. The coordinate reference frame is a two-dimensional cylindrical coordinate system taken over domain Ω . In the absence of body forces, the system of equations can be represented through the conservation of mass equation, as,

$$\nabla \cdot \mathbf{u} = 0, \quad (3.1)$$

the conservation of momentum transport equation, as,

$$\rho \frac{\partial \mathbf{u}}{\partial t} = \nabla \cdot \sigma - \rho \mathbf{u} \cdot \nabla \mathbf{u}, \quad (3.2)$$

where, \mathbf{u} is the fluid velocity vector field, σ is the Cauchy stress tensor, ρ is the fluid density, t represents time and ∇ the spatial differential operator. The Cauchy stress tensor can be expressed in the form:

$$\sigma = -p\delta + \mathbf{T}, \quad (3.3)$$

where p is the isotropic fluid pressure, δ is the Kronecker delta tensor, whilst \mathbf{T} is the total stress tensor. For constant viscosity (μ) Newtonian fluids, the stress tensor \mathbf{T} is given as

$$\mathbf{T} = 2\mu \mathbf{d}, \quad (3.4)$$

where the rate-of-strain tensor $\mathbf{d} = \frac{1}{2}[\nabla \mathbf{u} + (\nabla \mathbf{u})^\dagger]$, and \dagger represents the transpose operator.

Relevant non-dimensional Reynolds number is defined as:

$$Re = \frac{\rho V_c R}{\mu_c}, \quad (3.5)$$

The characteristic velocity V_c is taken to be the speed of the vessel, the characteristic length scale is the radius, R , of a stirrer and the characteristic viscosity μ_c is the zero shear-rate viscosity.

Appropriate scaling in each variable takes the form. At a characteristic rotational speed 50 rpm and zero shear viscosity of 105 Pa s, scaling yields dimensional variables $p = 2444p^*$.

4. NUMERICAL METHOD

As stated earlier, a time-marching finite element algorithm is employed in this investigation to compute numerical solutions through a semi-implicit Taylor-Galerkin /pressure-correction scheme [15], [21], [16]-[18], based on a fractional-step formulation. This involves discretisation, first in the temporal domain, adopting a Taylor series expansion in time and a pressure-correction operator-split, to build a second-order time-stepping scheme. Spatial discretisation is achieved via Galerkin approximation for the both momentum and stress constitutive equations. The finite element basis functions employed are quadratic (ϕ_j) for velocities, and linear (ψ_k) for pressure. Corresponding integrals are evaluated by a seven point Gauss quadrature rule.

Stage 1a:

$$\begin{aligned} \left[\frac{2\mathbf{M}}{\Delta t} + \frac{\mathbf{S}}{2Re} \right] (\mathbf{V}_r^{n+\frac{1}{2}} - \mathbf{V}_r^n) &= L_r^\dagger P^n - \frac{\mu_c}{Re} \{S_{rr} V_r + S_{r\theta} V_\theta\}^n \\ &- \{ \mathbf{N}(\mathbf{V}) V_r - N_1(V_\theta) V_\theta \}^n \end{aligned}$$

$$\begin{aligned} \left[\frac{2\mathbf{M}}{\Delta t} + \frac{\mathbf{S}}{2Re} \right] (\mathbf{V}_\theta^{n+\frac{1}{2}} - \mathbf{V}_\theta^n) &= L_\theta^\dagger P^n - \frac{\mu_c}{Re} \{S_{r\theta}^\dagger V_r + S_{\theta\theta} V_\theta\}^n \\ &- \{ \mathbf{N}(\mathbf{V}) V_\theta - N_1(V_\theta) V_r \}^n \end{aligned}$$

Stage 1b:

$$\begin{aligned} \left[\frac{2\mathbf{M}}{\Delta t} + \frac{\mathbf{S}}{2Re}\right](\mathbf{V}_r^* - \mathbf{V}_r^n) &= L_r^\dagger P^n - \frac{\mu_c}{Re} \{S_{rr}V_r + S_{r\theta}V_\theta\}^n \\ &\quad - \{\mathbf{N}(\mathbf{V})V_r - N_1(V_\theta)V_\theta\}^{n+\frac{1}{2}} \\ \left[\frac{2\mathbf{M}}{\Delta t} + \frac{\mathbf{S}}{2Re}\right](\mathbf{V}_\theta^* - \mathbf{V}_\theta^n) &= L_\theta^\dagger P^n - \frac{\mu_c}{Re} \{S_{r\theta}^\dagger V_r + S_{\theta\theta}V_\theta\}^n \\ &\quad - \{\mathbf{N}(\mathbf{V})V_\theta - N_1(V_\theta)V_r\}^{n+\frac{1}{2}} \end{aligned}$$

Stage 2:

$$\theta \mathbf{KQ}^{n+1} = \frac{1}{\Delta t} \mathbf{LV}^*,$$

Stage 3:

$$\frac{1}{\Delta t} \mathbf{M}(\mathbf{U}^{n+1} - \mathbf{U}^*) = -\theta \mathbf{L}^\dagger \mathbf{Q}^{n+1},$$

where \mathbf{V}^n are the nodal velocity vector at time t^n , respectively; \mathbf{V}^* is an intermediate non-divergence-free velocity vector, \mathbf{V}^{n+1} is a divergence-free velocity vector at time step t^{n+1} . \mathbf{P}^n is a pressure vector and $\mathbf{Q}^{n+1} = \mathbf{P}^{n+1} - \mathbf{P}^n$ is a pressure difference vector. \mathbf{M} is a mass matrix, $\mathbf{N}(\mathbf{V})$ is a convection matrix, \mathbf{K} is a pressure stiffness matrix, \mathbf{L} is a divergence/pressure gradient matrix and \mathbf{S} is a momentum diffusion matrix. Utilising implied inner product notation $\langle . \rangle$ for domain integrals, the above system involves matrices of the form:

Mass matrix:

$$\mathbf{M} = \int_{\Omega} \phi_i \phi_j r d\Omega,$$

Non-linear advection matrices:

$$\mathbf{N}(\mathbf{V}) = \int_{\Omega} \phi_i (\phi_l V_r^l \frac{\partial \phi_j}{\partial r} + \frac{\phi_l V_\theta^l}{\psi_k R_k} \frac{\partial \phi_j}{\partial \theta}) r d\Omega,$$

and

$$\mathbf{N}_1(V_\theta) = \int_{\Omega} \phi_i \phi_l V_\theta^l \phi_j r d\Omega, \text{ where } i, j, l = 1, \dots, 6$$

Pressure stiffness matrix:

$$\mathbf{K}_{km} = \int_{\Omega} \nabla \psi_k \nabla \psi_m r d\Omega, \text{ where } k, m = 1, 2, 3,$$

Pressure gradient matrix:

$$\mathbf{L}_{mi} = \int_{\Omega} \psi_m \nabla \phi_i r d\Omega$$

Momentum diffusion matrices:

$$\mathbf{S} = \begin{pmatrix} S_{rr} & S_{r\theta} \\ S_{r\theta}^\dagger & S_{\theta\theta} \end{pmatrix},$$

where \dagger is transpose of the matrix and

$$\begin{aligned}\mathbf{S}_{rr} &= \int_{\Omega} \left(2 \frac{\partial \phi_i}{\partial r} \frac{\partial \phi_j}{\partial r} + \frac{2 \phi_i \phi_j}{(\psi_k R_k)^2} + \frac{1}{(\psi_k R_k)^2} \frac{\partial \phi_i}{\partial \theta} \frac{\partial \phi_j}{\partial \theta} \right) r d\Omega \\ \mathbf{S}_{r\theta} &= \int_{\Omega} \left(\frac{1}{\psi_k R_k} \frac{\partial \phi_i}{\partial \theta} \frac{\partial \phi_j}{\partial r} + \frac{2 \phi_i}{(\psi_k R_k)^2} \frac{\partial \phi_j}{\partial \theta} - \frac{1}{(\psi_k R_k)^2} \frac{\partial \phi_i}{\partial \theta} \phi_j \right) r d\Omega, \\ \mathbf{S}_{\theta\theta} &= \int_{\Omega} \left(\frac{\partial \phi_i}{\partial r} \frac{\partial \phi_j}{\partial r} + \frac{\phi_i \phi_j}{(\psi_k R_k)^2} - \frac{1}{\psi_k R_k} \phi_i \frac{\partial \phi_j}{\partial r} - \frac{1}{\psi_k R_k} \frac{\partial \phi_i}{\partial r} \phi_j \right. \\ &\quad \left. + \frac{2}{(\psi_k R_k)^2} \frac{\partial \phi_i}{\partial \theta} \frac{\partial \phi_j}{\partial \theta} \right) r d\Omega.\end{aligned}$$

Repeated indices imply summation, taken over i , j and l for all velocity nodal points, and k , m for all vertex pressure nodal points on the triangular meshes. \mathbf{F}^n is a forcing function vector due to body force and boundary conditions at time t_n (which vanishes here). To give the precise second-order form of the pressure-correction algorithm the Crank-Nicolson coefficient θ is taken as one half. Stage one and three are governed by augmented mass matrices and solved by a Jacobi iterative method that necessitates using only a small fixed number of mass iterations, typically three. At stage two, a Poisson equation emerges, with a matrix that is symmetric and positive definite. It possesses a banded structure, for which it is appropriate to employ a direct Choleski method. The bandwidth may be optimised by using an algorithm such as that of Sloan [23]. Here, n denotes the time step index. Velocity components at the half time step $n + \frac{1}{2}$ are computed in step 1a from data gathered at level n and in step 1b an intermediate non-solenoidal velocity field \mathbf{V}^* is computed at the full time step, using the solutions at the level n and $n + \frac{1}{2}$.

For pressure this leads naturally to a second step, where a Poisson equation is solved for the pressure-difference from a non-solenoidal velocity field \mathbf{V}^* over the full time step. Solving for temporal pressure-difference has some specific advantages with respect to boundary conditions at the second step, see [15]. On a third and final step, a solenoidal velocity is captured at the end of the time-step cycle, computed from the pressure-difference field of step 2. For finite element approximation, the generalised weighting function w_i replaces ϕ_i , for the Galerkin formulation of momentum equation. In general, the time-step, Δt , is taken as 10^{-2} , so as to satisfy a local Courant Condition constraint [18]-[21] and a relative solution-increment time-step termination tolerance of 10^{-5} is enforced. The implicit splitting of pressure terms in the pressure correction leads to the factor θ , and a second-order scheme if taken as $\frac{1}{2}$. In addition, the Crank-Nicolson splitting of diffusion terms at stage-1, incorporates the implicit diffusion contribution to the left-hand-side of the equation.

5. NUMERICAL RESULTS

The numerical results are investigated from two distinct points of view: changing rotational speed and direction of stirrer. This leads to analysis with respect to increasing viscosity levels (decrease of Reynolds number) and comparison of flow structure and pressure variation across problem instances.

The predicted solutions are displayed for Newtonian fluid through contours plots of streamlines, and pressure isobars. Pressure isobar patterns are plotted with

eleven contours, from the minimum to maximum value, over a fixed range. Streamlines are plotted in two regions: first from the vessel wall to the stirrer perimeter, seven contours are plotted ($\Psi = 0, 0.5, 1.0, 1.5, 2.0, 2.5$ and 2.95 units) and second from the stirrer to the centre of the recirculation, $3.05 \leq \Psi \leq \Psi_{max}$ at increments of 0.3 units. Comparative diagnostics may be derived accordingly.

Various increasing levels of zero-shear viscosities μ_c (characteristic) are considered, from which Reynolds number is computed, as defined above. For Reynolds numbers of $Re = 8.0$, $Re = 0.8$ and $Re = 0.08$, the corresponding zero shear viscosities are $\mu_c = 1.05$ Pa s, $\mu_c = 10.5$ Pa s and $\mu_c = 105.0$ Pa s. Of these levels, a range of material properties is covered from those for model fluids, to model dough, to actual dough, respectively.

5.1. Flow Patterns and Pressure Differential for Stationary Stirrer with Increasing Inertia.

The effect of increasing Reynolds number upon streamline patterns on left and pressure differential on right isobars are represented in contour plots for stationary stirrer in figure-2. Computations are carried out at $Re = 0.08$, $Re = 0.8$ and $Re = 8$. At a low level of inertia, $Re = 0.08$, an intense recirculating region forms in the centre of the vessel, parallel to the stirrer and symmetrically intersecting the diameter that passes through the centres of the vessel and stirrer. Flow structure remains unaffected as Reynolds number rises to values of $O(1)$; hence we suppress this data. However, upon increasing Reynolds number up to eight, so $O(10)$, inertia takes hold and the recirculation region twist and shifts towards the upper-half plane, vortex intensity wanes and the vortex eye is pushed towards the vessel wall. The flow becomes asymmetric as a consequence of the shift in vortex core upwards. The diminishing trend in vortex intensity is tabulated in Table-1.

TABLE 1. Vortex intensity for Newtonian fluids: ($\mu_c = 105, 10.5$ and 1.05 Pas)

Problem	Speed	Re=0.08		Re=0.8		Re=8.0	
		<i>Min.</i>	<i>Max.</i>	<i>Min.</i>	<i>Max.</i>	<i>Min.</i>	<i>Max.</i>
Stationary Stirrer	Zero	0.00	5.091	0.00	5.087	0.00	4.852
Co-rotating stirrer	Double	0.00	10.259	0.00	10.294	0.00	11.482
	Same	0.00	7.295	0.00	7.299	0.00	7.299
	Half	0.00	7.295	0.00	7.295	0.00	7.295
Contra-rotating stirrer	Double	-2.884	2.865	-2.897	2.857	-3.913	2.171
	Same	0.00	3.734	0.00	3.731	0.00	3.557
	Half	0.00	4.340	0.00	4.340	0.00	4.160

Similar symmetry arguments apply across the geometry variants in pressure differential, at $Re = 0.08$, symmetric pressure isobars appear with equal magnitude in non-dimensional positive and negative extrema on the two sides (upper and lower) of the stirrer in the narrow-gap. As inertia increases from $Re = 0.8$ to $Re = 8$, asymmetric isobars are observed, with positive maximum on the top of the stirrer and negative minimum at the outer stirrer tip (near the narrow-gap), see also Table-2.

Asymmetrical flow structure is observed in all variables and across all instances as inertia increase from $Re = 0.08$ to $Re = 8.0$, recirculating flow-rate decrease by just five percent. In non-dimensional terms above $Re = 0.08$ (noting scale differences), there is increase in pressure-differential rise by as much as twenty-two percent, at $Re = 8.0$, whilst pressure differential increase on the lower part of the stirrer. For Newtonian fluid, the extrema of recirculating region along with vortex intensity and pressure differential, are tabulated for completeness in Tables (1 and 2) at all three Reynolds number values.

5.2. Flow Patterns And Pressure Differential For Co-Rotating Stirrer With Increasing Inertia. Equivalent field kinematic data for co-rotating stirrer with increasing Reynolds number from $Re = 0.08$ to $Re = 8.0$ is presented in figure-3, to make direct comparisons across all instances for Newtonian fluids, with particular reference to localised vortex intensity and pressure drops are tabulated in Tables (1 and 2).

In figure-3(i), for co-rotating case, stream lines are shown for decreasing speed of the stirrer (from left to right), double speed (left), same speed (centre) and half speed (right), only single vortex is formed, in contrast to the contra rotating case where three vortices were formed, see figure 4(i). At $Re = 0.08$, doubling the speed of the stirrer the vortex is formed near to the stirrer and is much more circular and smooth in formation, but as the speed of the stirrer is reduced to half the vortex moves away from the stirrer towards the right and the centre of the vortex is circular on one side and on other side is suppressed, also showing an increase space between the centre of vortex and diameter of secondary streamline. Streamlines tend to increase in density at the edges of the stirrer. At $Re = 0.8$, the centre of the recirculating region is shifted towards the lower-half of the plane. The diameter of the vortex also increases and leaves no circulation of fluid in the centre of recirculating region. At $Re = 8.0$, the shape of the vortex centre is changed and further shifted towards the lower half of the plane. At the half speed of the stirrer and $Re = 8.0$, the shape of the recirculating region is changed and vortex centre amplifies in the size. Consequently, the fluid pushes towards vessel wall and create vacuum in the centre of the vessel.

For co-rotating instances, figure-3(ii) illustrates the pressure differential at all comparable parameter values. The pressure differentials are high and is about five times in negative extrema compare to stationary stirrer, at $Re = 8$ and small change is observed in positive maxima. Reducing the speed of stirrer from double to single speed, the pressure differentials is very low and remain in order of two for all inertial values. Subsequently, further reduction in the speed of stirrer to half virtually no change in the pressure differential is observed and remain unaltered for all Reynolds numbers values, see Table-2.

5.3. Flow Patterns and Pressure Differential for Contra-Rotating Stirrer with Increasing Inertia. Corresponding field kinematics data for contra-rotating stirrer situation with increasing Reynolds number at $Re = (0.08, 0.8$ and $8.0)$ the streamline contours and pressure differentials are presented in figure-4(i and ii) respectively. In figure-4(i), for contra-rotating case, streamlines are illustrated for decreasing speed of the stirrer from double (left) to half (right) against the speed of vessel the three vortices develops, two in the vicinity of stirrer, one in narrow gap and other in middle of the vessel, and third in the centre of vessel away from stirrer

TABLE 2. Pressure drop for Newtonian fluids: ($\mu_c = 105, 10.5$ and 1.05 Pas)

Problem	Speed	Re=0.08		Re=0.8		Re=8.0	
		<i>Min.</i>	<i>Max.</i>	<i>Min.</i>	<i>Max.</i>	<i>Min.</i>	<i>Max.</i>
Stationary Stirrer	Zero	-3.366	3.356	-3.421	3.325	-5.117	3.541
Co-rotating stirrer	Double	-5.234	4.916	-6.734	3.987	-26.117	4.924
	Same	-1.631	1.553	-1.984	1.209	-1.984	1.209
	Half	-1.984	1.209	-1.984	1.209	-1.984	1.209
Contra-rotating stirrer	Double	-11.578	11.380	-12.479	10.498	-28.358	6.906
	Same	-7.443	7.384	-7.719	7.127	-11.808	5.272
	Half	-5.394	5.372	-5.394	5.372	-8.218	4.849

close to vessel wall. In the narrow gap, where stirrer spins in counter direction of the vessel rotation, a small vortex appear with low vortex intensity, as the speed of stirrer decrease this vortex strength up to fifty percent high at low $Re = 0.08$. The augmentation in minima of vortex intensity is observed with increase in inertia, however, it suppress in maxima of vortex intensity. As inertia takes hold the second and third recirculation regions shifts the centres towards the upper-half plane of the vessel. For all Reynolds number values at double speed of stirrer, the central vortex rotate in counter direction against two other vortices. These recirculation regions have different rotational direction which is very important phenomena in homogenisation of the fluid.

For all three instances, comparable equilibrium influence apply across the geometry variants in pressure differential, at $Re = 0.08$ and double rotational speed of stirrer, symmetric pressure isobars appear with equal magnitude in non-dimensional positive and negative extrema on both sides (upper and lower) of the stirrer in the narrow-gap as shown in figure-4(ii). The associated values of pressure differentials are tabulated in Table-2. As inertia increase from $Re = 0.8$ to $Re = 8$, asymmetric isobars are observed, with positive maxima on the top of the stirrer and negative minima at the outer stirrer tip (near the narrow-gap), see also Table-3. For the contra-rotating instance, in contrast to co-rotating case, the pressure differentials are some what symmetrical in geometry at maxima and minima at twice the speed of stirrer and at half the speed of stirrer for both inertial values $Re = 0.08$ and $Re = 0.8$. However, upon increasing Reynolds number up to eight, thus $O(10)$, inertia takes hold the pressure differentials are observed asymmetrical, increasing the speed of the stirrer to double increases the pressure differentials more than twice in negative minima and in contrast it decrease up to thirty five percent in positive maxima. Comparing against co-rotating case at same double speed of stirrer increase in minima is merely eight percent and increase in maxima is about thirty percent.

6. CONCLUSIONS

The use of a numerical flow simulator as a prediction tool for this industrial flow problem has been successfully demonstrated. We have been able to provide

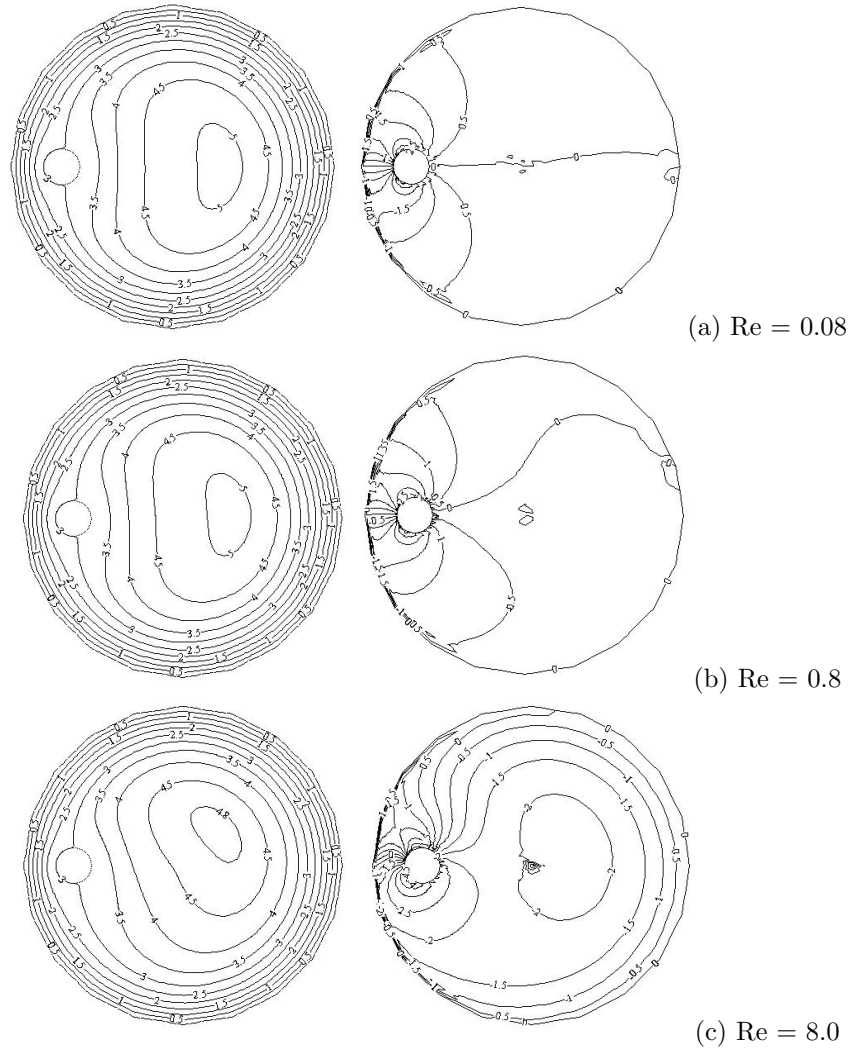


FIGURE 2. Streamline contours and pressure isobars of stationary stirrer with increasing Reynolds number.

physically realistic simulations for this complex mixing process using Newtonian fluid.

Addressing the rotation of the single stirrer case against stationary stirrer case in contra-rotating and co-rotating directions are being investigated with increasing inertia. For stationary stirrer case, it is clearly demonstrated that with increasing inertia fluid flow structure lose its symmetry and recirculating region move upwards in the direction of vessel motion and non-dimensional pressure differential increases. For co-rotating stirrer case, single recirculating region develops in the centre of the vessel and fluid suppressed towards vessel wall and leave big vacuum in the centre of the vessel. Whilst at twice the speed of stirrer pressure differentials are higher and lower at lower speed of stirrer. In contrast to these cases, contra-rotating case flow

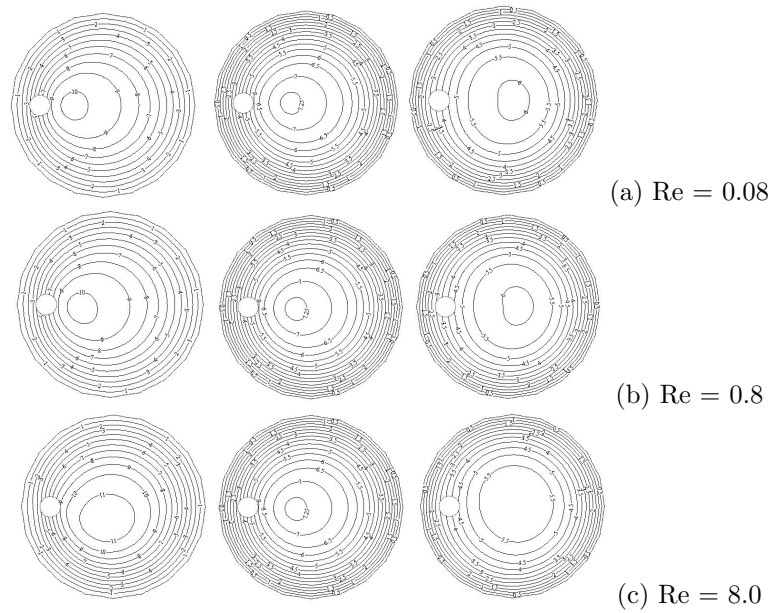


FIGURE 3(i). Streamline contours for co-rotating stirrer case with decreasing speed of the stirrer from left to right (double ($V_\theta = 2$), same ($V_\theta = 1$) and half speed ($V_\theta = 0.5$)) against speed of vessel and increasing Reynolds number.

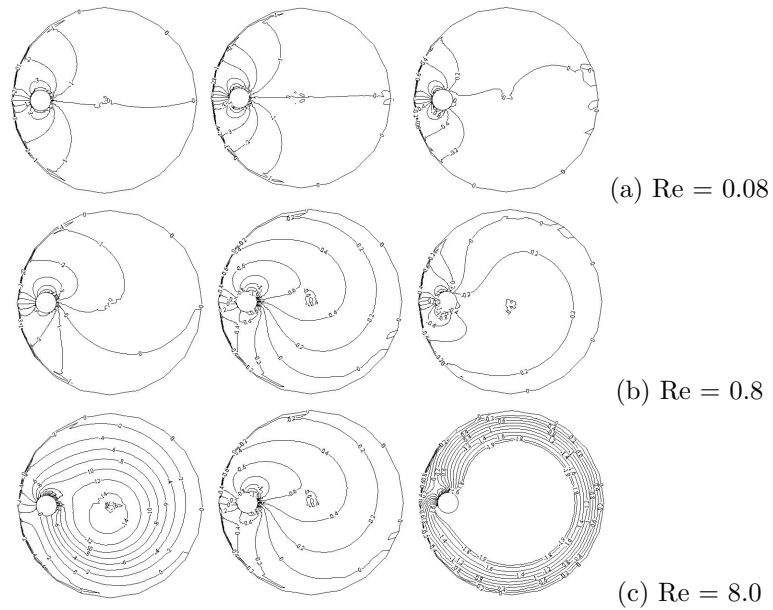


FIGURE 3(ii). Pressure isobars for co-rotating stirrer case with decreasing speed of the stirrer from left to right (double ($V_\theta = 2$), same ($V_\theta = 1$) and half speed ($V_\theta = 0.5$)) against speed of vessel and increasing Reynolds number.

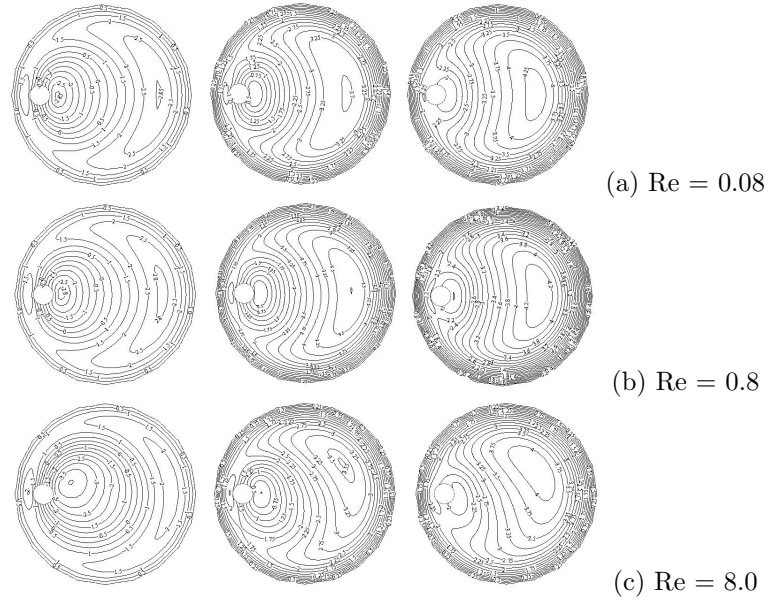


FIGURE 4(i). Streamline contours for co-rotating stirrer case with decreasing speed of the stirrer from left to right (double ($V_\theta = 2$), same ($V_\theta = 1$) and half speed ($V_\theta = 0.5$)) against speed of vessel and increasing Reynolds number.

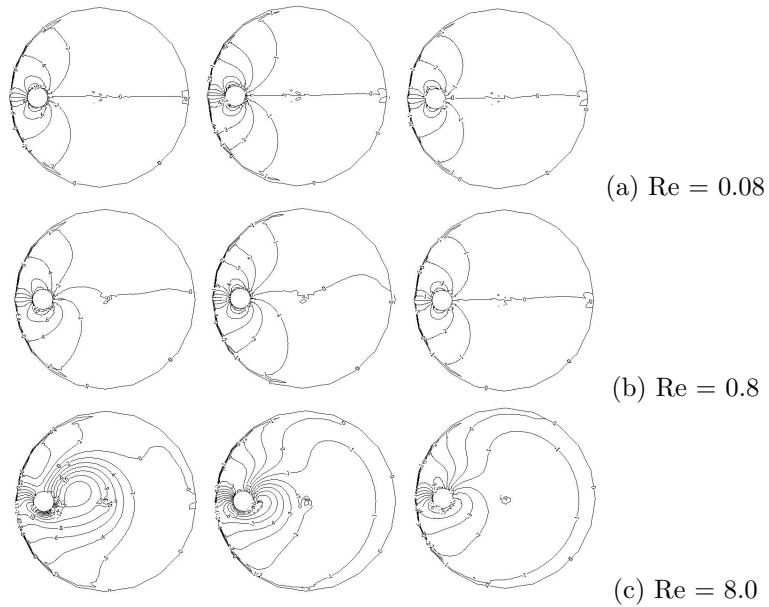


FIGURE 4(ii). Pressure isobars for co-rotating stirrer case with decreasing speed of the stirrer from left to right (double ($V_\theta = 2$), same ($V_\theta = 1$) and half speed ($V_\theta = 0.5$)) against speed of vessel and increasing Reynolds number.

structure and pressure differential illustrates completely different picture. Instead of single vortex three recirculating regions have been developed with different position of vortex centres. The pressure differentials are generally higher, and similar balance in extrema is noted to those flows. However, the position, in those negative maxima exceeds to positive minima by about four times. Through the predictive capability generated, we shall be able to relate this to mixer design that will ultimately impact upon the processing of dough products.

Promising future directions of this work are investigation of rotation of two stirrers case in co-rotating, contra-rotating and mixed rotating directions, changing material properties using non-Newtonian fluids and introducing agitator in concentric configured stirrer.

ACKNOWLEDGEMENT

The authors are greatly acknowledged to the Mehran University of Engineering and Technology, Jamshoro, for providing computational facility.

REFERENCES

- [1] P. M. Portillo, F. J. Muzzio, and M. G. Ierapetritou, *Hybrid DEM-Compartment Modelling Approach for Granular Mixing*, AIChE Journal, **53** (1) (2007), 119-128.
- [2] N. Phan-Thien, M. Newberry and R. I. Tanner, *Non-linear oscillatory flow of a solid-like viscoelastic material*, J. Non-Newtonian Fluid Mech., **92** (2000), 67-80.
- [3] K. S. Sujatha, M. F. Webster, D. M. Binding, M. A. Couch, *Modelling and experimental studies of rotating flows in part-filled vessels: wetting and peeling*, J. Foods Eng., **57** (2002), 67-79.
- [4] D. M. Binding, M. A. Couch, K. S. Sujatha, M. F. Webster, *Experimental and numerical simulation of dough kneading in filled geometries*, J. Foods Eng., **57**, (2002), 1-13.
- [5] K. Sujatha, D. Ding, M. F. Webster, *Modelling three-dimensions mixing flows in cylindrical-shaped vessels*, in: ECCOMAS CFD - 2001, Swansea, UK, (2001), 1-10.
- [6] K. Sujatha, D. Ding, M. F. Webster, *Modelling of free surface in two and three dimensions*, in: C. A. Brebbia, B. Sarlen (Eds.), Sixth International Conference on Computational Modelling of Free and Moving Boundary Problems - 2001, WIT, Lemnos, Greece, (2001), 102-111.
- [7] D. Ding, M. F. Webster, *Three-dimensional numerical simulation of dough kneading*, in: D. Binding, N. Hudson, J. Mewis, J.-M. Piau, C. Petrie, P. Townsend, M. Wagner, K. Walters (Eds.), XIII Int. Cong. on Rheol., Vol. 2, British Society of Rheology, Cambridge, UK, (2000), 318-320.
- [8] A. Baloch, P. W. Grant and M. F. Webster, *Parallel Computation of Two-Dimensional Rotational Flows of the Viscoelastic Fluids in Cylindrical Vessel*, Int. J. Comp. Aided Eng. and Software, Eng. Comput., **19** (7) (2002), 820-853.
- [9] A. Baloch, and M. F. Webster, *Distributed Parallel Computation for Complex Rotating Flows of Non-Newtonian Fluids*, Int. J. Numer. Meth. Fluids, **43** (2003), 1301-1328.
- [10] I. Dris and S. G. Shaqfeh, *On purely elastic instabilities in eccentric cylinder flows*, J. Non-Newtonian Fluid Mech., **56** (1995), 349-360.
- [11] I. Dris and S. G. Shaqfeh, *Flow of a viscoelastic fluid between eccentric cylinders: on flow stabilities*, J. Non-Newtonian Fluid Mech., **80** (1998), 59-87.
- [12] X. K. Li, D. R. Gwynllyw, A. R. Davies, T. N. Phillips, *On the influence of lubricant properties on the dynamics of two-dimensional journal bearings*, J. Non-Newtonian Fluid Mech., **93**, 1, (2000), 29-59.
- [13] Tanner, R. I., *Engineering Rheology*, 2nd Edition, Oxford University Press, Oxford, 2000.
- [14] R. G. Larson, *Constitutive Equations for Polymer Methods and Solutions*, Butterworths, 1988.
- [15] Townsend, P. and Webster, M. F., *An algorithm for the three-dimensional transient simulation of non-Newtonian fluid flows*, in: G. Pande, J. Middleton (Eds.), Proc. Int. Conf. Num. Meth. Eng.: Theory and Applications, NUMETA, Nijhoff, Dordrecht, pp. T12/1-11, 1987.

- [16] Carew, E. O., Townsend, P. and Webster, M. F., *Taylor-Petrov-Galerkin algorithm for viscoelastic flow*, J. Non-Newtonian Fluid Mech., **50** (1994), 253-287.
- [17] Baloch, A., Townsend, P. and Webster, M. F., *On the highly elastic flows*, J. Non-Newtonian Fluid Mech. **59** (1995), 111-128.
- [18] H. Matallah, P. Townsend, M. F. Webster, *Recover and stress-splitting schemes for viscoelastic flows*, J. Non-Newtonian Fluid Mech., **75** (1998), 139-166.
- [19] N. Phan-Thien, R. I. Tanner, *A new constitutive equation derived from network theory*, J. Non-Newtonian Fluid Mech., **2** (1977), 353-365.
- [20] S. W. Sloan, *An algorithm for profile and wave-front reduction of sparse matrices*, Int. J. Num. Meth. Eng., **23** (1986), 239-251.
- [21] D. M. Hawken, H. R. Tamaddon-Jahromi, P. Townsend, M. F. Webster, *A Taylor-Galerkin-based algorithm for viscous incompressible flow*, Int. J. Num. Meth. Fluids, **10** (1990), 327-351.
- [22] R. B. Bird, W. E. Stewart, E. N. Lightfoot, *Transport Phenomena*, Wiley International Edition, 1960.
- [23] T. Cochrane, K. Walters, M. Webster, *On Newtonian and non-Newtonian flow in complex geometries*, Phil. Trans. R. Soc. London, **A308** (1982), 163-181.
- [24] W. J. Lunsman, L. Genieser, R. C. Armstrong, R. A. Brown, *Finite element analysis of steady viscoelastic flow around a sphere in a tube: calculations with constant viscosity models*, J. Non-Newtonian Fluid Mech., **48** (1993), 63-99.
- [25] N. Phan-Thien, *A non-linear network viscoelastic model*, J. Rheology, **22(3)** (1978), 259-283.
- [26] R. Keunings, *Parallel finite element algorithms applied to computational rheology*, Comp. Chem. Engg., **19 (6-7)**(1995), 647-669.
- [27] H. S. Dou, N. Phan-Thien, *Parallelisation of an unstructured finite volume code with pvm: viscoelastic flow around a cylinder*, J. Non-Newtonian Fluid Mech., **77(1-2)**(1997), 21-51.
- [28] A. Baloch, P. W. Grant and M. F. Webster, *Homogeneous/Heterogeneous Distributed Cluster Computation of Two and Three-Dimensional Viscoelastic Flows*, Int. J. Numer. Meth. Fluids, **40** (2000), 1347-1363.